Proceedings of the 17th World Congress
The International Federation of Automatic Control
Seoul, Korea, July 6-11, 2008

# Damping Path Design for Liquid Container Transferred with Wheeled Mobile Robot along Multiple Turn Sections

**Yu Yoshida*, Masafumi Hamaguchi** and Takao Taniguchi*****

** Department of Electronic and Control Systems Engineering, Graduate School of Shimane University, Shimane, Japan ( e-mail: s069802@matsu.shimane-u.ac.jp)*
*** Department of Electronic and Control Systems Engineering, Shimane University, Shimane, Japan ( e-mail: hamaguchi@ecs.shimane-u.ac.jp)*
**** Department of Electronic and Control Systems Engineering, Shimane University, Shimane, Japan ( e-mail:taniguchi@ecs.shimane-u.ac.jp)*

**Abstract:** This paper proposes a design method of a damping path for a cylindrical liquid container transferred with a wheeled mobile robot. The damping path is constructed from the acceleration using the principle of an input shaping method. Although a positional error is occurred by using the input shaping method, it is easy to correct the error with the proposed method. The proposed design method can be applied to a complex reference path including multiple turn sections. In addition, a constraint condition of maximum amplitude of sloshing in the container can be taken into consideration. The effectiveness of the proposed method is clarified through simulations and experiments.

## 1. INTRODUCTION

With the advancement of automation at various factories, liquid container transfers have become very important processes in production lines. For example, there are transfers of molten metals, transfers of molds after pouring as part of material processing in steel and casting industries, or transfers of raw material solutions and mixed solutions in chemical plants without using pipes. In such processes, containers have generally no lid to speed up and simplify pouring works. In liquid container transfers, sloshing (liquid vibration) is generated by changes in the container's acceleration. Overflows and degradation of quality caused by sloshing in containers are problems that directly affect productivity. For instance, there is the degradation by the contamination of air and slag in transfers of molten metals. In addition, production processes are shifting to job shop type productions recently.

In transportation systems, transfer paths are often changed to deal with the change of processes. Wheeled mobile robots (WMRs) are more useful than belt conveyer or rail systems in terms of the easiness on path changes. Moreover, the adverse effect on a carrier such as a collapse and sloshing in transfer can be reduced by a path design without adding any control devices.

Liquid container transfer using robot arms, cart or vehicles are studied (J.T. Feddema *et al.* [1997], K. Yano *et al.* [2001], T. Acarman and U. Ozquner [2003]). In those papers, although damping the sloshing is discussed, damping path design and trace control are not considered. Path planning and trace control for WMRs have been studied (W.H. Wu *et al.* [2000], M.L. Corradini and G. Orlando [2001]). However, there are few studies on the liquid container transfer using WMR. We previously reported a damping path design for a cylindrical liquid container on WMR using an input shaping method (M. Hamaguchi and T. Taniguchi [2005]). In that paper, a way to design damping paths for only simple reference paths was proposed, but this way is inconvenient to design complex paths including multiple turn sections.

This paper proposes a damping path design of a liquid container on WMR using the input shaping method. The present method can easily handle both paths including multiple turn sections and constraint conditions of maximum amplitude of sloshing. The usefulness of this method is demonstrated through simulations and experiments.

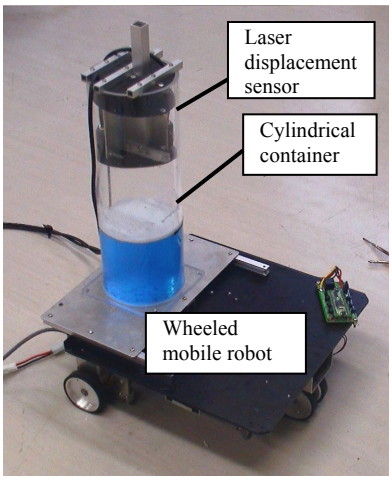


Fig.1. Experimental equipment

## 2. EXPERIMENTAL EQUIPMENT

The liquid in the cylindrical container is transferred with the wheeled mobile robot as shown in Fig. 1. The robot is the tricycle type which consists of two driving wheels and one steering wheel. These wheels are driven by DC motors. The

rotational speed of the right and left driving wheels are measured by means of rotary encoders, and the steering angle is done by a potentiometer. The steering wheel is adjusted using a PID controller in order to work as a caster. This steering system improves straightness and steering above those of common casters. The driving wheels are driven using a PID controller to obtain the desired speed.

The container is mounted on the mobile robot. The inner diameter of the container is 0.10 m, its height is 0.30 m. Water is chosen as the target liquid because of its simplicity of handling and low cost. Liquid level is 0.10 m. Two laser displacement sensors are used to observe the liquid level at the front measuring point and the left side one. The water is colored with a blue paint and plastic powder is floated so that the laser sensors can detect the water surface.

## 3. MODEL EQUATIONS

Model equations of sloshing are described for the design of a transfer control system. When the mass of the container with the liquid is sufficiently heavier than that of the robot, pitching and rolling motions may be taken into consideration in the model equations of the robot and sloshing. The terms of these motions, here, are omitted from the model equations.

### *3.1 Wheeled mobile robot*

A schematic representation of the wheeled mobile robot is shown in Fig. 2. Disregarding slipping of the wheels, the kinematic model equations of the robot are shown as follows:

$$\dot{x}_r = v\cos\theta_r, \quad \dot{y}_r = v\sin\theta_r, \quad \dot{\theta}_r = \omega, \tag{1}$$

$$v = \frac{v_r + v_l}{2}, \quad \omega = \frac{v_r - v_l}{2d}, \tag{2}$$

$$\tan\phi_r = \frac{b}{r}, \quad r = \frac{v}{\omega}, \tag{3}$$

where $x_r$, $y_r$ means the position of the axle center $O_r$ on $X$-$Y$ plane, $v$ is the velocity of the axle center $O_r$, $\theta_r$ is the direction of the robot, $\omega$ is the angular velocity around the vertical axis of the robot, $v_r$ and $v_l$ are the circumferential speeds of the wheels of right and left, respectively, $2d$ is the distance between driving wheels, $b$ is the wheelbase, $\phi_r$ is the steering angle, and $r$ is the curvature radius of the path. The position $x_r$, $y_r$ and the direction $\theta_r$ are determined by the circumferential speeds of the right and left wheels, $v_r$ and $v_l$. These values of $v_l$, $v_r$ and $\phi_r$ are controlled with appropriate PID controllers. Assuming that the time constant of the robot is sufficiently decreased with these controllers, here, the dynamics of the robot is disregarded.

The model equations of the driving wheels are given as a first-order delay system:

$$\left.\begin{aligned} \dot{v}_r &= -\frac{1}{T_w}v_r + \frac{K_w}{T_w}u_r, \\ \dot{v}_l &= -\frac{1}{T_w}v_l + \frac{K_w}{T_w}u_l, \end{aligned}\right\} \tag{4}$$

where $u_r$ and $u_l$ are the input voltages to the wheels of right and left, respectively, $T_w$ is the time constant, and $K_w$ is the gain.

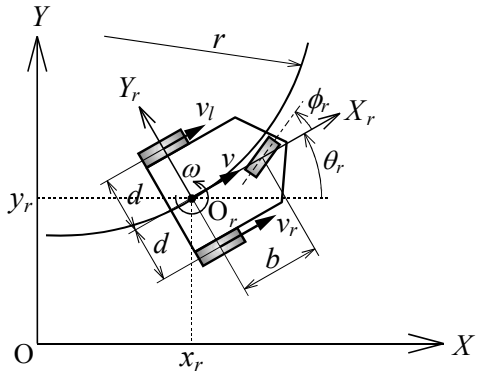


Fig. 2. A schematic representation of the WMR

### *3.2 Sloshing*

The spherical pendulum-type sloshing model (M. Hamaguchi and T. Taniguchi [2005]) is shown in Fig. 3. The sloshing model approximately expresses (1, 1)-mode sloshing, which is a dominant mode of sloshing in the case of container transfer excluding intense vibrations. In this model, the liquid surface is considered to be the plane perpendicularly installed on the pendulum. That is to say, the sloshing has been replaced with the motion of the pendulum. The equations of the sloshing model are obtained as follows:

$$\left.\begin{aligned} \ddot{\theta} &= -\frac{g\sin\theta}{\ell\sin\phi} + 2\dot{\theta}\dot{\phi}\tan\phi + 2\dot{\phi}\frac{v}{r}\cos\theta \\ &\quad + \frac{v^2}{r^2}\sin\theta\cos\theta - \frac{c_\theta}{m}\dot{\theta}\cos^2\theta \\ &\quad + \frac{c_\theta}{m}\sin\theta\cos\theta\tan\phi \\ &\quad + \dot{v}\cos\theta\left(\frac{\tan\phi}{r} - \frac{1}{\ell\cos\phi}\right), \\ \ddot{\phi} &= -\frac{g\sin\theta}{\ell\sin\phi}2\dot{\theta}\dot{\phi}\tan\theta\sin^2\phi \\ &\quad - 2\dot{\theta}\frac{v}{r}\cos\theta\cos^2\phi - \frac{v^2}{\ell r}\cos\phi \\ &\quad + 2\dot{\phi}\frac{v}{r}\sin\theta\sin\phi\cos\phi \\ &\quad + \left(\frac{v^2}{r^2} - \dot{\theta}^2\right)\sin\phi\cos\phi \\ &\quad - \frac{c_\phi}{m}\dot{\phi}\cos^2\phi - \frac{\dot{v}}{r}\sin\theta\cos^2\phi \\ &\quad - \ddot{\theta}\tan\theta\sin\phi\cos\phi, \end{aligned}\right\} \tag{5}$$

where $\theta$ is the angle of the pendulum mapped onto the $z$-$x$ plane, $\phi$ is the angle between the original pendulum and the mapped pendulum, $g$ is the gravitational acceleration, $\ell$ is the equivalent length of the pendulum, $m$ is the mass of the liquid, and $c_\theta$ and $c_\phi$ are the equivalent coefficients of viscosity for sloshing on $\theta$ and $\phi$, respectively. The displacement of the liquid level $h_x$ at the front measuring point and $h_y$ at the left side measuring point are described as

$$h_x = L\tan\theta, \quad h_y = \frac{L\tan\phi}{\cos\theta}, \tag{6}$$

where $L$ is the distance between the measuring point and the center of the container. Equations (5) and (6) are linearized by using a linear approximation technique and some assumptions (M. Hamaguchi and T. Taniguchi [2005]) in order to create a linear control system, because the above nonlinear model is too complicated to allow for the design of a control system. The linearized equations are as follows:

$$\left.\begin{aligned} \hat{\theta} &= -\frac{g}{\ell}\theta - \frac{c_\theta}{m}\dot{\theta} - \frac{\dot{v}}{\ell}, \\ \ddot{\phi} &= -\left(\frac{g}{\ell} - \frac{v^2}{r^2}\right)\phi - \frac{c_\phi}{m}\dot{\phi} - \frac{v^2}{\ell r}, \end{aligned}\right\} \tag{7}$$

$$h_x = L\theta, \quad h_y = L\phi. \tag{8}$$

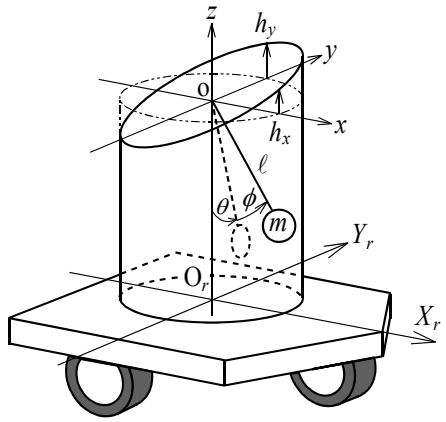


Fig. 3. Spherical pendulum-type sloshing model

## 4. DESIGN OF DAMPING TRANSFER PATH

An input shaping method is applied to running and centripetal acceleration of the robot to damp the sloshing in the container. A damping path is constructed according to the shaped acceleration.

### *4.1 Input Shaping Method*

An input shaping method (N.C. Singer and W. P. Seering [1990]) is adopted for the transfer control system. The principle of the two-impulse input technique is illustrated in Fig. 4. The vibration caused by the unit impulse input of the acceleration is canceled by the following impulse input that has amplitude of $k$ and time delay of $\Delta T$. When the transfer function is a linear second order system given as (9), $\Delta T$ and $k$ can be analytically formulated as (10),

$$G(s) = \frac{K\omega_n{}^2}{s^2 + 2\zeta\omega_n s + \omega_n{}^2}, \tag{9}$$

$$\Delta T = \frac{\pi}{\omega_n\sqrt{1-\zeta^2}}, \quad k = \exp\left(\frac{-\zeta\pi}{\sqrt{1-\zeta^2}}\right), \tag{10}$$

where $\omega_n$ is the system's natural angular frequency, $\zeta$ is the damping ratio, and $K$ is the gain.

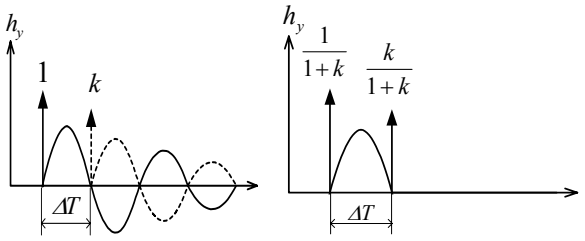


(a) Response without the shaping method (b) Response with the shaping method

Fig. 4. Two-impulse input technique in input shaping method

### *4.2 Design of damping path*

From (7) and (8), transfer functions from running acceleration $\dot{v}$ to $h_x$ and from centripetal acceleration $v^2/r$ to $h_y$ are same type as (9), respectively. Therefore the input shaping method can be applied for designing damping path. The method of the path design has three steps. The details of that are described in the following.

#### *4.2.1 Temporary reference path*

When a start point, a goal point and passing points are given, a temporary reference path is designed with straight lines and circular arcs as shown in Fig. 5. Curvature radius $R_A$ should be larger than the minimal turning radius of the robot. Transfer speeds $v$ in all sections are decided by a designer.

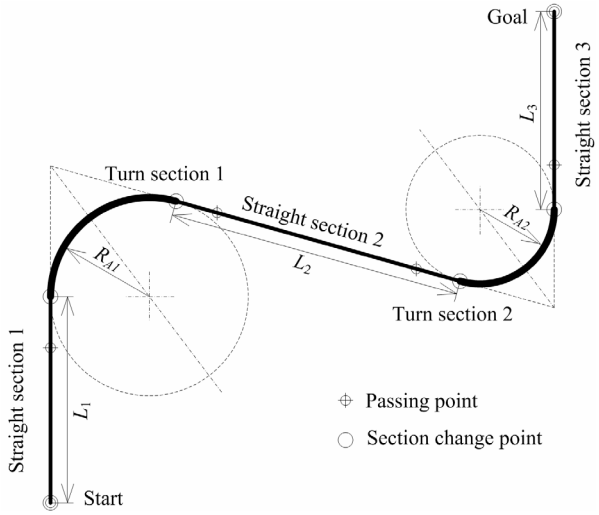


Fig. 5. Temporary reference path

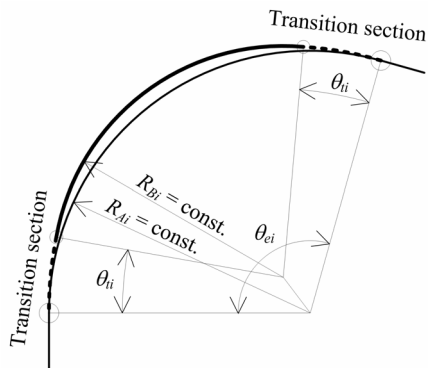


Fig. 6. The i-th curve section of nominal reference path

*4.2.2 Nominal reference path*

The robot cannot run along the temporary reference path because acceleration, deceleration and curvature transition sections are not taken into consideration in the path. Acceleration, deceleration and curvature transition sections should be added to the temporary reference path. The acceleration or deceleration sections are carried out only in straight sections, which means the transfer speed $v$ is constant in the turn sections for the simplification of the damping path design. Curvature transition sections are inserted into the beginning and the end of the turn section as shown in Fig. 6, where $\theta_e$ is a turning angle. The curvature linearly changes in the transition sections. The transition section has a transition angle $\theta_t$ as shown in Fig. 6. The curvature should be zero at the connecting point of straight and turn section for smooth connecting. In other words, the path of the transition section is a clothoid curve. Positions of both ends in each turn section should be unchangeable in spite of the transition sections. It is comfortable to design the path because of this condition. To realize this condition, curvature radius $R_B$ must be smaller than $R_A$. Curvature radius $R_B$ is calculated from (11), which is obtained by using a solver of Mathematica.

$$\begin{aligned} R_{Bi} = {} & 5.40\times10^3 R_{Ai} \Big/ \left(-3.60\times10^3\theta_t^{\,2} + 2.57\times10^2\theta_t^{\,4}\right. \\ & -8.19\theta_t^{\,6} + 0.143\theta_t^{\,8} + \cot\theta_e/2\cdot\left(-1.08\times10^4\theta_t\right. \\ & \left.\left.+1.08\times10^3\theta_t^{\,3} - 50.1\theta_t^{\,5} + 1.16\theta_t^{\,7}\right)\right. \\ & \left.+5.41\times10^3\csc\theta_t/2\cdot\sin\left(\theta_t-\theta_e/2\right)\right) \end{aligned} \tag{11}$$

*4.2.3 Damping path*

The damping path is designed based on the nominal reference path. The running and centripetal accelerations of the robot are calculated from the nominal reference path. The damping path is obtained with applying the input shaping method to these accelerations. The input shaping method is applied to the running acceleration and the centripetal acceleration, respectively. The damping path is obtained by means of twice integrating the accelerations. However, positional errors occur in the damping path as shown in Fig. 7. The lengths of the straight paths are adjusted to correct the positional errors in the straight sections. It is difficult to correct the positional errors in the curved sections. Because the turn sections consist of two or more clothoid curves, the equations of the positional errors become complex. The correction is simplified by using the characteristics of the damping path applied the input shaping method. Two characteristics of the positional error for the centripetal acceleration are shown below.

(C1) The positional error caused by the input shaping method is almost unchangeable in spite of the transition section.
(C2) The change of the positional error according to the change of the curvature radius can be disregarded.

(C1) is useful to form the equation of the positional error briefly. (C2) lets us decide the revised curvature radius to correct the positional error without troublesome procedures. The positional errors $\Delta X$ for $x$-direction and $\Delta Y$ for $y$-direction are obtained as (12) and (13), respectively.

$$\begin{aligned} \Delta X_i = {} & kR_{Ai}\left\{1-\cos\left(\frac{v\Delta T}{R_{Ai}+kR_{Ai}}\right)\right\} \\ & +\frac{R_{Ai}}{k}\left\{\cos\left(\frac{kv\Delta T}{R_{Ai}+kR_{Ai}}-\theta_{ei}\right)-\cos\theta_{ei}\right\} \end{aligned} \tag{12}$$

$$\begin{aligned} \Delta Y_i = {} & kR_{Ai}\sin\left(\frac{v\Delta T}{R_{Ai}+kR_{Ai}}\right) \\ & +\frac{R_{Ai}}{k}\left\{\sin\left(\frac{kv\Delta T}{R_{Ai}+kR_{Ai}}-\theta_{ei}\right)-\sin\theta_{ei}\right\} \end{aligned} \tag{13}$$

The curvature radius $R_A$ in (11) is replaced with $R'_A$ of (14). When $R_B$ calculated by using $R'_A$ is used in the nominal reference path, there is no positional error in the curved section of the damping path.

$$R'_{Ai} = \frac{R_{Ai}\left(1-\cos\theta_{ei}\right)-\Delta X_i}{1-\cos\theta_{ei}} \tag{14}$$

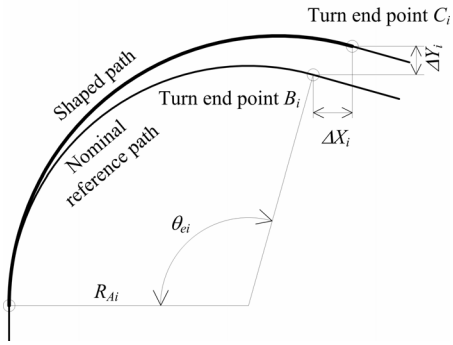


Fig.7. Positional error caused by the input shaping method

The procedure of designing the damping path is summarized as follows.

(P1) Design the temporary reference path with the start point, goal point and passing points.
(P2) Design the nominal reference path with the acceleration, deceleration and transition sections.
(P3) Replace the curvature radius $R_A$ in (11) with the revised curvature radius $R'_A$ of (14).
(P4) Adjust the beginning positions of the turn sections from (12) and (13).
(P5) Apply the input shaping method to the revised nominal

reference path.

## 5. SIMULATION AND EXPERIMENTAL RESULTS OF DAMPING TRANSFER

Figure 8 shows the designed damping path. The parameters values for turn sections are indicated in Table 1. In this case, although $\pi$ rad or $\pi/2$ rad is used as the turning angle $\theta_e$, $\theta_e$ can be arbitrary angle. The length of each straight section is $L_{1,\,2,\,\cdots,\,6}$ = 0.300, 0.300, 0.200, 0.300, 0.200, 0.300 (m), and the transfer speed is 0.5 m/s. Table 2 shows other parameter values. The non-revised damping path does not pass through all the passing points. On the other hand, the revised damping path passes through all passing points. Figure 9 shows the running and centripetal acceleration in Fig. 8.

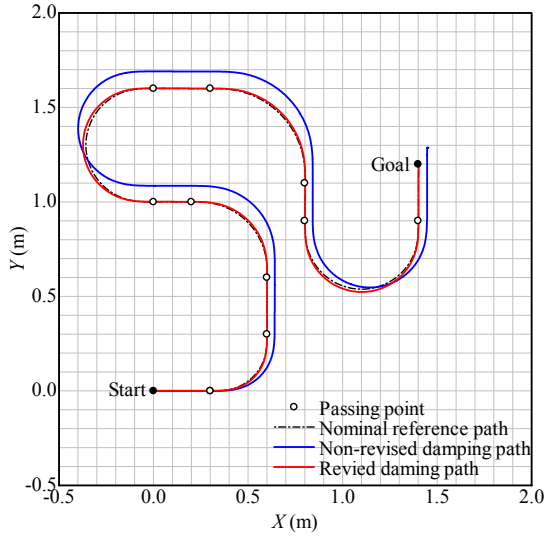


Fig. 8. Designed damping path

Table 1. Parameters values for turn sections

| $i$ | $R_{Ai}$ (m) | $\theta_{ei}$ (rad) | $\theta_{ti}$ (rad) | Turning direction |
|---|---|---|---|---|
| 1 | 0.300 | $\pi/2$ | $\pi/15$ | CCW |
| 2 | 0.400 | $\pi/2$ | $\pi/25$ | CCW |
| 3 | 0.300 | $\pi$ | $\pi/15$ | CW |
| 4 | 0.500 | $\pi/2$ | $\pi/30$ | CW |
| 5 | 0.300 | $\pi$ | $\pi/15$ | CCW |

Table 2. Parameters values for damping path design

| | | | |
|---|---|---|---|
| $\ell$ (m) | 0.0253 | $T_w$ (s) | 0.550 |
| $m$ (kg) | 0.785 | $2d$ (m) | 0.249 |
| $c_\theta$, $c_\phi$ (Ns/m) | 1.27 | $b$ (m) | 0.235 |
| $L$ (m) | 0.0360 | $\Delta T$ (s) | 0.160 |
| $K_w$ (m/(sV)) | 0.179 | $k$ (-) | 0.899 |

Figure 10 shows the simulation results of the transfer through the damping path. The sloshing is occurred in the nominal reference path. There is no residual vibration in the revised damping path. The adverse effect on the damping performance due to revising is not completely observed in the results.

The experimental results of the transfer through the damping path are shown in Fig. 11. These results a little differ from the simulation results because of the adverse effect of the running plane with ruggedness and swell. In spite of it, the damping effect is obtained obviously by using the damping path.

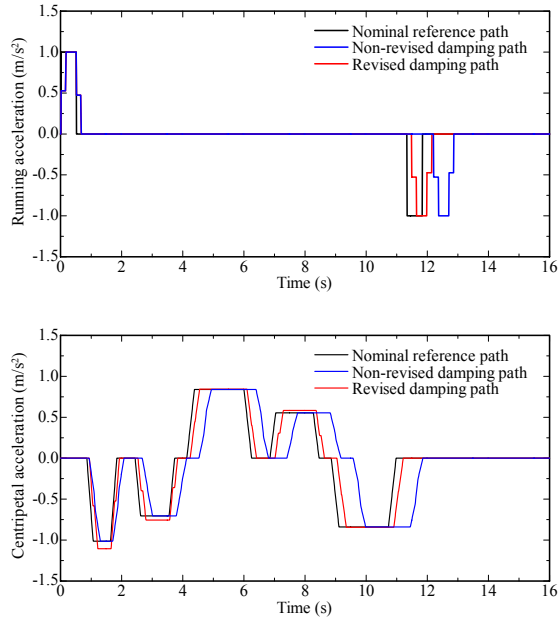


Fig. 9. Acceleration on designed damping path

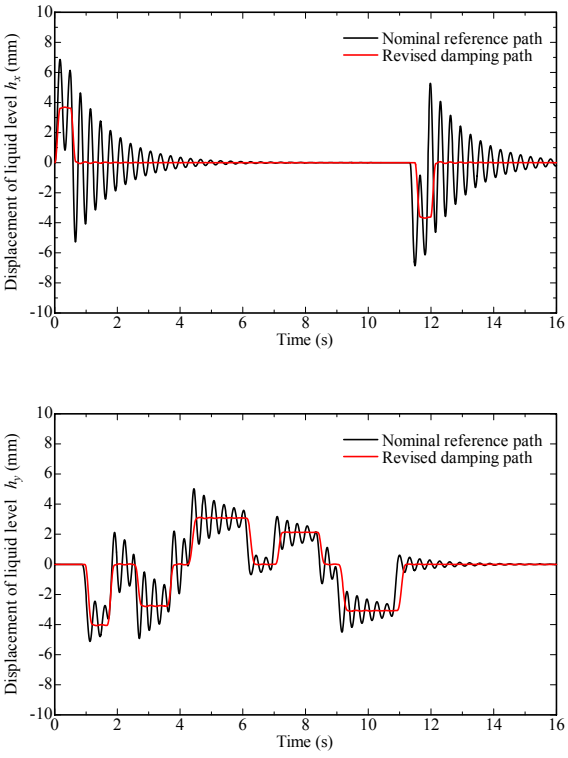


Fig. 10. Simulation results of damping transfer

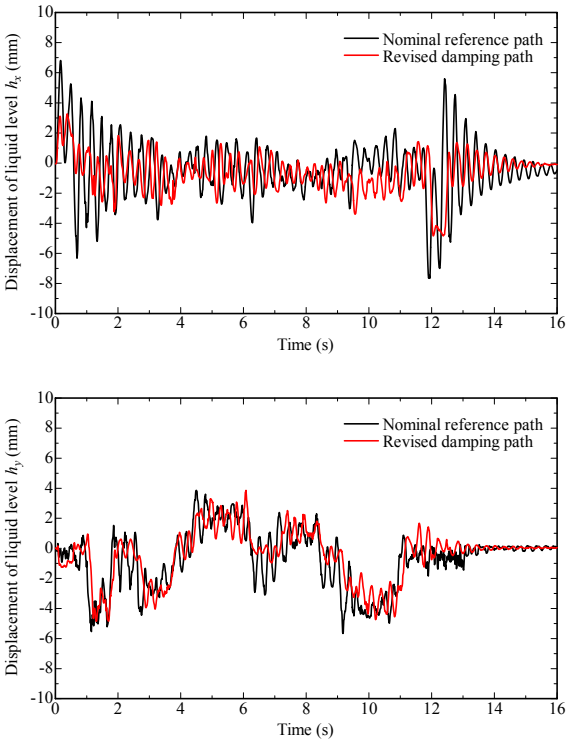


Fig. 11. Experimental results of damping transfer

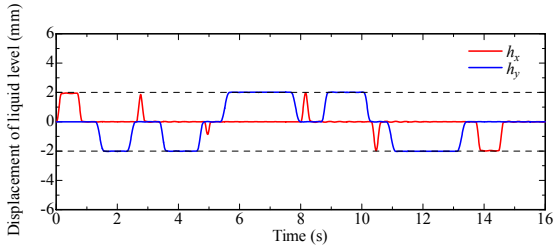


Fig. 12. Simulation results of damping transfer with constraint condition $h_{\lim}$=2 (mm)

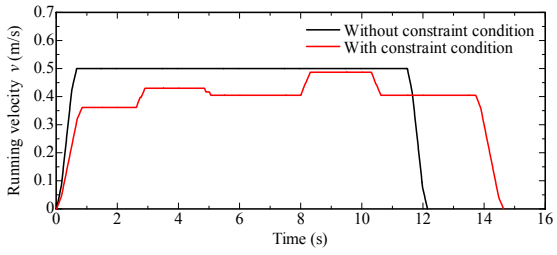


Fig. 13. Running velocity corresponding to Fig. 12

Maximum amplitudes of sloshing for $h_x$ and $h_y$ are calculated as follows:

$$h_{x_{\max}} = L\frac{\dot{v}}{g}, \quad h_{y_{\max}} = L\frac{v^2/R_B}{g}. \tag{15}$$

If limit amplitude of sloshing $h_{\lim}$ as a constraint condition is given, it is possible to satisfy a condition $h_{x,y_{\max}} = h_{\lim}$ by adjusting the transfer velocity $v$ in the straight sections. When any $v$ is given, $h_{y_{\max}}$ are calculated from (11) - (15). The desired velocity $v^*$ as $h_{y_{\max}} = h_{\lim}$ can be simply obtained by using a bisection method for $f(v) = h_{y_{\max}}(v, R_B(v)) - h_{\lim} = 0$. Maximum running acceleration $\dot{v}_{\max}$ is restricted from (15) so that $h_{x_{\max}}$ may be equal to $h_{\lim}$. The simulation results of damping transfer with the constraint condition of $h_{\lim}$=2 (mm) are shown in Fig. 12. The constraint condition is satisfied obviously. Figure 13 shows the result of running velocity corresponding to Fig.12. It is proven that the constraint condition is satisfied by adjusting the running velocity.

## 6. CONCLUSION

In this paper, a design method of damping path including multiple turn sections has been realized by using an input shaping method. A method to correct positional errors has been proposed. In addition, a constraint condition on maximum amplitude of sloshing can be taken into consideration by adjusting transfer velocity in straight sections. It is notable that the proposed damping transfer can be constructed with an open loop control for sloshing and has a sufficient damping effect to damp sloshing. In the proposed method, it is easy to change a damping path, because a reference path can be divided into some sections and the calculating time for redesigning a damping path is very short. Therefore, even if a robot encounters unexpected obstacles on the way, it is possible to redesign the local part of the damping path immediately.

## REFERENCES

T. Acarman and U. Ozquner [2003]. Rollover Prevention for Heavy Trucks Using Frequency Shaped Sliding Mode Control. *Proceedings of 2003 IEEE Conference on Control Applications*, **Vol. 1**, pp. 7-12.

M.L. Corradini and G. Orlando [2001]. Robust Tracking Control of Mobile Robots in the Presence of Uncertainties in the Dynamical Model. *Journal of Robotic Systems*, **Vol. 18**, **No. 6**, pp. 317-323.

J.T. Feddema *et al.* [1997]. Control for Slosh-Free Motion of an Open Container. *IEEE Control Systems Magazine*, **Vol. 17**, **No. 1**, pp. 29-36.

M. Hamaguchi and T. Taniguchi [2005]. Damping and Transfer Control of Liquid in a Cylindrical Container Using a Wheeled Mobile Robot. *Journal of Robotics and Mechatronics*, **Vol. 17**, **No. 5**, pp. 546-552.

N.C. Singer and W. P. Seering [1990]. Preshaping Command Inputs to Reduce System Vibration. *ASME Journal of Dynamic Systems, Measurement, and Control*, **Vol. 112**, pp. 76-82.

W.H. Wu *et al.* [2000]. Time Optimal Path Planning for a Wheeled Mobile Robot. *Journal of Robotic Systems*, **Vol. 17**, **No. 11**, pp. 585-591.

K. Yano *et al.* [2001]. Sloshing Suppression Control of Automatic Pouring Robot by Hybrid Shape Approach. *Proceedings of the 40th IEEE Conference on Decision and Control*, **Vol. 2**, pp. 1328-1333.